ELSEVIER

Polymer 40 (1999) 7397–7407

polymer

Processing and microstructural characterization of porous biocompatible protein polymer thin films

Christopher J. Buchko[a,*], Loui C. Chen[a], Yu Shen[a], David C. Martin[a,b]

[a]*Department of Materials Science and Engineering, University of Michigan, Ann Arbor, MI 48109, USA*
[b]*Macromolecular Science and Engineering Center, University of Michigan, Ann Arbor, MI 48109, USA*

Received 1 June 1998; received in revised form 25 November 1998; accepted 10 December 1998

Abstract

The process of electrostatic fiber formation, or electrospinning, was used to create biocompatible thin films for use in implantable devices. The morphology of the thin films was found to depend on process parameters including solution concentration, applied electric field strength, deposition distance, and deposition time. The microstructure of the coatings was examined by Transmission Electron Microscopy (TEM) and Wide-Angle X-ray Scattering (WAXS), with electrospun filaments being weakly oriented along the fiber axis. A shish kebab model for the filament morphology was proposed. The electrospinning process was shown to be a means of creating porous thin films with structural gradients and controlled morphology that could enhance biocompatibility.

Keywords: Electrospinning; Protein polymers; Microstructure

1. Introduction

A new class of biomaterials was synthesized using recombinant DNA biosynthesis technology [1]. These protein polymers combine amino acid sequences found in natural silk with amino acid sequences that correspond to biofunctional fragments found in extracellular matrix proteins such as fibronectin and laminin. The rationale behind this combination was to create a biologically active material that could be processed into useful structures by virtue of the thermal and the chemical stability of the crystalline silk-like segments. This article discusses an electrostatic fiber formation method used to deposit a Silk-Like Polymer with Fibronectin functionality (SLPF) as a thin film onto prosthetic devices designed to be implanted in the Central Nervous System (CNS).

Thin films can be deposited on implantable devices in order to facilitate the integration of these devices with the body. A useful coating design would contain both functional and structural gradients to encourage cellular ingrowth and reduce the mechanical mismatch between the device and the tissue as well as a surface structure that could help integrate the device into the body [2]. The surface structure of the coating is primarily a function of macroscopic morphology, while mechanical properties can depend on both macroscopic structure and the nature and extent of the crystalline microstructure. To this end, the influence of processing variables on macroscopic coating morphology and microstructure is evaluated.

1.1. Processing

SLPF and its related polypeptides are easily processed from solvents including formic acid, hexafluoroisopropanol, and lithium bromide/acetic acid [3]. These solvents enable the protein polymers to be processed at room temperature or under a variety of conditions. Nonsolvents include methanol, acetone, and water. A careful selection of the solvent, nonsolvent, and the means of precipitating the protein polymer from a solution has created a number of structures including films, fibers, coatings, and foams [4–7]. This flexibility enables the development of solution-processing schemes for depositing coatings of protein polymers onto biomedical devices. Parameters that determine the properties of the solution-processed product are concentration, viscosity, evaporation rate, and the presence of a nonsolvent.

The process described in this article is that of electrostatic fiber formation, or electrospinning. Electrospinning is a special case of electrostatic atomization, a process that was explored in detail by Zeleny in 1917 [8]. Michelson [9] provides an excellent overview of the electrostatic

* Corresponding author. Corresponding address: Guidant Corporation, 3200 Lakeside Drive, Santa Clara, CA 95054, USA. Tel.: 001-408-235-3363; fax: 001-408-235-3648.

0032-3861/99/$ - see front matter
PII: S0032-3861(98)00866-0

atomization theory and modern applications. Electrostatic atomization occurs when the surface tension of a liquid is overcome by an applied electric field, thereby ejecting tiny droplets from the surface. Polymeric solutions behave differently compared to monomeric liquids during electrostatic atomization in that they persist as elongated jets over a much greater distance.

Taylor [10] identified the critical electric potential for electrostatically forming a cone of liquid (now known as a Taylor cone) at the end of a capillary tube. The derivation began with the expression for the equilibrium state of a droplet at the end of a pressurized tube, and the coefficients for the electrostatic potential were generated by observing the deflection of charged solutions at the end of an inverted capillary, giving:

$$V_c^2 = 4\frac{H^2}{L^2}\left(\ln\frac{2L}{R} - \frac{3}{2}\right)(0.117\pi\gamma R), \quad (1)$$

where V_c is the critical voltage, H, the separation between the capillary and the ground, L, the length of the capillary, R, the radius of the capillary, and γ, the surface tension of the liquid. A similar relationship was developed by Hendricks et al. [11] for the potential required for the electrostatic spraying from a hemispherical drop pendant from a capillary tube:

$$V = 300\sqrt{20\pi\gamma r}, \quad (2)$$

where r is the radius of the pendant drop [11]. In each case, the conducting drop was assumed to be surrounded by air, and suspended in a stable position from the capillary tube. These equations are appropriate physical models for droplet formation for slightly conducting, monomeric fluids. By examining a small range of fluids Taylor determined that a 49.3° equilibrium angle balanced surface tension with electrostatic forces, and used this value in his derivation. However, it was shown that conductivity and viscosity both play vital roles in the electrostatic atomization process, and can influence the equilibrium angle and other aspects of the process [9]. The dependence on conductivity and viscosity is missing from these two equations, but the relationship between surface tension and applied voltage serves as a useful guide for slightly conducting, medium-to-low viscosity solutions. Taylor cones are important to electrospinning in that they define the onset of extensional velocity gradients in the fiber forming process [12]. Other important aspects of electrospinning which were examined include analysis of the different modes of droplet formation as a function of several process variables [13] and the scale-up of atomization using a linear array of Taylor cones [14].

There is precedent for the application of electrostatic atomization techniques to polymeric solutions in the patent and academic literature. Included among the relevant patents are schemes for creating biomedical products such as wound dressings and vascular grafts [15,16]. In addition to these patents, there are studies of electrospinning processes that evaluate the influence of process variables such as solution viscosity, polymer concentration, and applied field strength on the morphology of the resulting polymer fibers [12,17–21].

A wide variety of synthetic and natural polymers are electrospun from solution [17,18,20,21] and poly(propylene) and poly(ethylene) were electrospun from the melt [12]. Submicron fibers, as small as tens of nanometers, were electrospun from solution [17,19,21], while melt-spun fibers were on the order of tens to hundreds of microns [12]. Submicron fibers of protein polymers were electrospun in our laboratory [5–7]. A fibrous material was obtained by applying an electric field to an aqueous dilute solution of silk fibroin [22]. In all these processes, splaying of the fiber during electrospinning generated a range of fiber diameters during each spinning process.

Solution parameters were correlated with fiber morphology by all three groups. Baumgarten [17] determined the limits of spinnability for a poly(acrylonitrile)/DMF solution and also observed a dependence of the fiber diameter, d, on solution viscosity, η such that:

$$d \approx \eta^{0.5}. \quad (3)$$

Larrondo and Manley [12] observed that the fiber diameter decreased with increasing melt temperature. Given the relationship between melt temperature and viscosity, they were able to draw a qualitative correlation between diameter and viscosity. Doshi [19] identified an inverse relationship between molecular weight and concentration for spinnability of poly(ethylene oxide) in aqueous solutions, but did not correlate changes in viscosity with fiber diameter. An observation was made that, jet breakup depends on viscosity so that lower viscosity solutions break up into droplets more readily. Thus, the solution or melt viscosity was shown to affect both the processing window for electrospinning and the diameter of the fibers.

Electric field parameters were also correlated with fiber morphology. Larrondo and Manley [12] determined that doubling the applied electric field decreased the fiber diameter by roughly half. However, Baumgarten [17] showed that the diameter of the jet reached a minimum after an initial increase in field strength and then became much larger with increasing fields. This effect was caused by the feed rate of the polymer solution through the capillary, and illustrates one of the complexities of the electrospinning process. That is, increasing the field does increase the electrostatic stresses, creating smaller diameter fibers, but it also draws more material out of the syringe. Doshi [19] plotted the jet diameter at different positions along the jet to verify both of these relationships. At the capillary orifice, there was a threefold increase in the jet diameter with less than a twofold increase in applied voltage. Also, in each study it was shown that increasing the applied field resulted in an increased spinning rate. Baumgarten [17], Doshi [19], and Reneker and Chun [21]

observed that low separation distances between the capillary and the ground resulted in wet fibers collecting at the target.

It is important to note that Larrondo and Manley [12], Doshi [19], and Reneker and Chun [21] paid attention to the strain rates in the spinning jet. The presence of elongational flow fields during the electrospinning of polymeric solutions is critical for orienting the polymer molecules along the fiber axis. Larrondo and Manley [12] determined the strain rate in their system to be on the order of $1\ s^{-1}$, while Reneker and Chun [21] have reported strain rates as high as $10^4\ s^{-1}$. The former rate was more than the molecular relaxation rate, preventing elongation of the molecule in the fiber direction, while the latter rate was high enough to induce molecular orientation.

1.2. Microstructure

SLPF was designed to mimic the fundamental amino acid sequence of natural silk. While many details of the microstructure of natural silk and polypeptide analogs of silk are still not known, two phases, Silk I and Silk II, dominate the discussion [23,24]. Silk I crystals were obtained by casting solubilized natural silk fibroin from solution at room temperature [25,26]. The addition of mechanical stresses to the system can produce the Silk II crystal structure. X-ray diffractions of Silk I and Silk II revealed distinct characteristic reflections [27]. However, both structures have a strong reflection near 0.45 nm, corresponding to the (1 1 0) planes in Silk I and the (0 2 0) planes in Silk II. Crystalline forms of SLPF were observed to be consistent with a model of Silk I [28].

Anderson et al. [28] used transmission electron microscopy (TEM) to demonstrate that atomized droplets of SLPF crystallized into whiskers with a fundamental width of 11.8 nm that correlated to the energy-minimized length of the silk-like repeat unit. This information led to a model for SLPF crystallites in which the silk-like repeat unit promotes crystallization and presents the fibronectin segments at the crystal surface. Dry SLPF powder was examined by Wide Angle X-Ray Scattering (WAXS), and as a function of exposure to a solvent/nonsolvent vapor system of formic acid and water [29]. It was determined that the 0.74 nm (0 2 0) correlations, which correspond to packing between hydrogen-bonded sheets, were disrupted first as the concentration of formic acid in the vapor was increased. As more solvent was added the intensity of the 0.45 nm (2 1 0) peak decreased, which corresponded to the disruption of correlations in the hydrogen-bonding direction. This result suggested that crystallization may also occur in stages, which has implications for processing the powder into products with a crystalline microstructure. Estimates of the per cent crystallinity as a function of solvation would have shed more light onto the solution-crystallization kinetics.

Electrospinning was investigated as a means of processing both amorphous and oriented crystalline submicron fibers from polymer solutions and polymer melts. Reneker and Chun [21] have reported the electrospinning of poly(esters) and poly(aramids) into oriented fibers from solution. The orientation was a result of the high elongational flow fields that the electrospinning apparatus exerted on these readily crystallizable or lyotropic liquid crystalline polymers. No descriptions of the resulting orientation of the other synthetic polymers or biopolymers electrospun with this apparatus were presented. Baumgarten [17] electrospun poly(acrylonitrile) from solution, but did not characterize the molecular orientation of the fibers. Molten polymers such as poly(propylene) and poly(ethylene) were electrospun into single filaments between 50 and 200 μm in diameter [12]. The fibers had an unoriented, spherulitic structure, except in the case of 1% poly(ethylene) in paraffin. These fibers displayed a fibrillar crystal structure reminiscent of a shish kebab morphology that can be correlated with an extensional velocity gradient in the flow field. Jaeger et al. [30] used scanning probe microscopy (SPM) to evaluate the surface morphology of electrospun poly(ethylene oxide) fibers. Their process created “beads-on-a-string” morphologies where, the fibers displayed oriented birefringence and the beads were spherulitic. The SPM images presented some evidence that the chain direction of the molecules was parallel to the fiber direction. Electron diffraction would have been superior for determining molecular alignment, but this SPM data did show an oriented texture on the surface of these submicron fibers.

SLPF was processed into submicron fibers by both electrospinning and vapor phase web casting [5–7]. The vapor phase technique relied on high shear rates generated by spraying a solution of SLPF in formic acid through a nozzle under a dry nitrogen atmosphere [7]. The resulting fibers were collected on targets and analyzed by TEM. Typical electron or X-ray diffraction patterns of polymer fibers have semi-arcs along the equator that correspond to lateral packing of extended chains extended along the fiber axis. It was not clear from the data whether the periodicities observed in the vapor phase fibers were because of longitudinal or lateral correlations in the filaments [7]. However, in WAXS of SLPF powder the strongest reflections were associated with lateral chain correlations [28]. In describing the electrospinning process and a vapor phase web casting technique, it was asserted that small fiber diameters would promote molecular alignment [7]. While this effect may be important in fibers with diameters less than the typical radius of gyration of a polymer coil (about 10 nm), for larger filaments it will likely be necessary to generate extensional flow fields to obtain a substantial orientation.

The results of these experiments and the prior work on the crystal structure of SLPF have important implications for the prospect of inducing crystallinity and molecular orientation in electrospun filaments [28,29]. Dry, as-received SLPF powder was crystalline, and an atomized dilute solution produced crystallites. In addition, the ability to form fibers by spraying suggests that hydrodynamic shear forces may

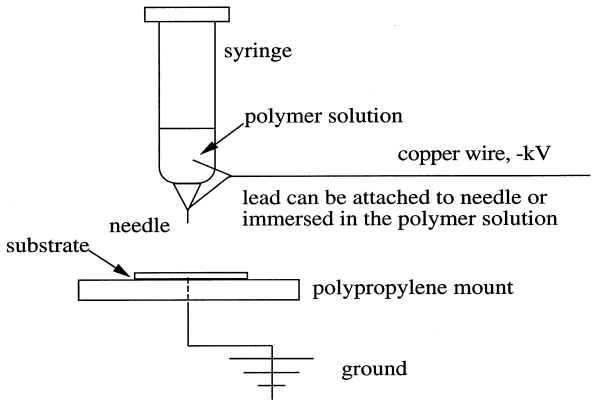

Fig. 1. Schematic of the electrospinning apparatus. The electric potential can be applied to the metal needle or directly to the solution by running the electrode through the syringe.

augment electrostatic forces to promote molecular orientation while electrospinning. Finally, the use of a dry nitrogen atmosphere for vapor phase web casting illustrates a means to control evaporation rates during fiber formation [7].

2. Experimental

2.1. Samples

Solutions were prepared the same day by dissolution in 96% formic acid (Aldrich). Typical mixing times varied with concentration, from 1 h at 0.8 wt.% to 4 h at 16.2 wt.%. Extrusion-grade nylon 6,6 (Monsanto) in formic acid was used as a model solution because of its rheological similarity to SLPF [6]. At the typical electrospinning concentrations of 0.8–16.2 wt.%, SLPF has a viscosity of 0.002–0.1 Pa s and nylon has a viscosity of 0.005–0.2 Pa s. Up to 20 wt.% water was added to some of these solutions to test the effect of water on the electrospinning process. Diced silicon wafers were used as substrates in place of the micromachined silicon devices. Thin glass coverslips were also used as substrates, as well as other nonconductive materials such as polypropylene suture and silicone rubber tubing.

2.2. Processing

The electrospinning apparatus consisted of a syringe barrel, a metal needle, and a grounded target (Fig. 1). The syringe barrel was filled with the polymer solution, which could be dispensed in regular increments using a repeating dispenser (Hamilton No. 83700). A voltage was applied to the solution by attaching the metal needle (ID 152 μm) to the voltage source, a Hipotronics 12 kV DC power supply. The ground lead was attached to a copper wire flush-mounted in a polypropylene sheet, and the silicon target was placed in contact with this wire. The applied field, deposition distance, solution concentration, and deposition time were all varied. Typical conditions included an applied field of 2–8 kV/cm, a deposition distance of 0.5–4 cm, a solution concentration of 0.8–16.2 wt.%, and a deposition time of 1–10 s. The deposition took place in air at room temperature.

2.3. Characterization

Optical Microscopy (OM) was performed on a Nikon Optiphot T2-POL polarized light microscope in both transmission mode and reflected light mode (bright and dark field). A 530 nm full wave plate, a six-order quartz wedge, and a Michel-Lévy Color Chart were used to determine the sign and magnitude of the birefringence. Flow birefringence measurements used a modular focusing mount for the Nikon objective lenses, polarizing sheets, and a conventional white light source. Real time images of the electrospinning process were recorded with a horizontal mount for an optical microscope nose-piece and video camera.

SPM data were collected using a Nanoscope III with Multimode Head (Digital Instruments) in both contact and tapping modes. The deposition rates were calculated from the SPM data, using the maximum thickness and mean thickness of the films. Film thickness was determined by scratching the coatings with a stylus mounted on a Teledyne–Taber Scratch Tester and examining the profile using SPM. Additional film thickness measurements were made using a WYKO RST Plus Optical Profilometer.

For examination in the Scanning Electron Microscope (SEM) samples were prepared by prepumping for 2 h to remove residual solvent and then sputtering a thin layer (∽5 nm) of Au/Pd onto them (Technics Hummer VI) to reduce electron charging effects. SEM was performed using a Hitachi S-800, operating in high vacuum at 2 kV. Fiber and bead morphology was quantitatively evaluated directly from negatives and by NIH image 1.58–1.6.

TEM (JEOL 2000 FX) samples were prepared by electrospinning solutions onto carbon coated mica. The thin carbon film (∽10 nm) was subsequently floated off onto deionized water and lifted onto copper grids. These TEM samples were occasionally coated with a thin layer of gold to improve contrast and provide an internal calibration standard for electron diffraction, and images were captured under conditions consistent with the reported Total End Point Dose (TEPD) for SLPF [28] of 0.02 C/cm^2.

Low dose TEM techniques [31] are those that minimize the exposure of the sample to the electron beam. Searching for sections of the sample suitable for imaging was typically done with the beam diverged so as to be much larger than the screen. When a section was identified as suitable for imaging, it was translated a small amount away from the beam and conditions appropriate for imaging were set. The sample was then translated back into the beam path and photo plates were taken.

Samples for WAXS were prepared by electrospinning solutions onto silicon and glass substrates and examined using a Bragg–Brentano goniometer with a Rigaku Rotaflex

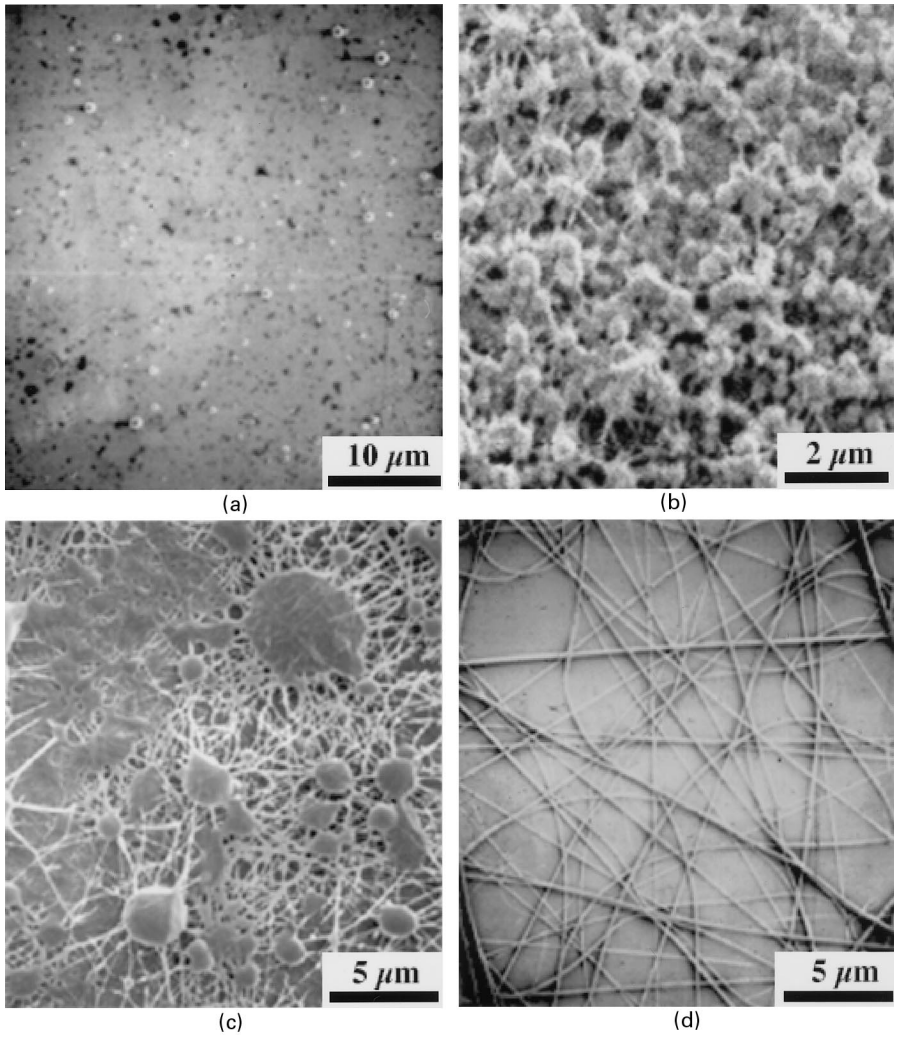

Fig. 2. Series of electrospun SLPF coatings where the polymer concentration in formic acid was varied: (a) 0.8 wt.%, (b) 4.1 wt.%, (c) 8.1 wt.%, (d) 12.1 wt.%.

rotating anode source operating at 40 kV and 100 mA. Samples for fiber diffraction were electrospun onto silicon substrates, removed using a razor blade, and placed in a flat-film Furnas camera attached to a sealed-tube source operating at 40 kV and 20 mA. The sample-to-film distance was 5 cm and the exposure time was typically 12–24 h.

3. Results and discussion

3.1. Processing

The processing parameters for electrospinning included concentration, deposition distance, applied field strength, and deposition time. The discontinuous thin films that were created by this process were composed of shaped elements such as fibers or beads. The aspects of the film structure which were affected by changing electrospinning process parameters included element shape, element size, and overall film thickness.

The morphology of the electrodeposited coatings changed as the concentration of SLPF in formic acid was varied. Fig. 2 shows a series of SEM micrographs showing the morphology changing from a beaded coating to a filamentous coating, with filamentous/beaded intermediate stages. All other parameters were kept constant at 4 kV/cm and 2 cm deposition distance. The change in morphology from beads to fibers was a result of a combination of phenomena related to the increase in concentration. Taylor [10] observed that in a monomeric fluid, lower viscosity resulted in the breakup of the electrically driven jet into individual droplets. The lowest concentration protein polymer solutions were deposited as individual droplets. An increase in polymer concentration from 0.8 to 4.1 wt.% resulted in droplets with filamentous asperities, or “hairy beads”. At this concentration, the polymer solution evidently responded to the local changes in electrostatic stresses on the surface of each droplet. These stresses deformed the individual droplets in the same way that the pendant droplet was deformed by the initial applied field [12]. At even

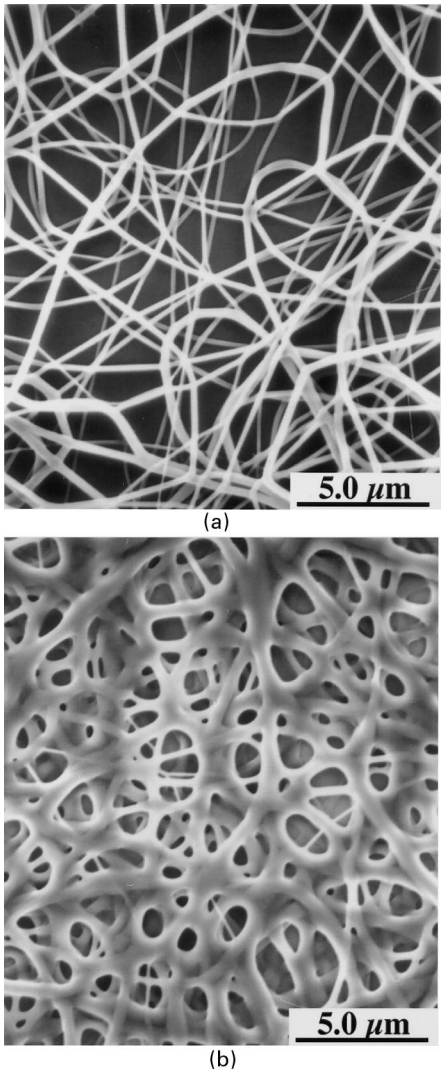

Fig. 3. Deposition distance controls morphology: (a) deposited at 2.0 cm, resulting in round fibers, (b) deposited at 0.5 cm, resulting in flat fibers.

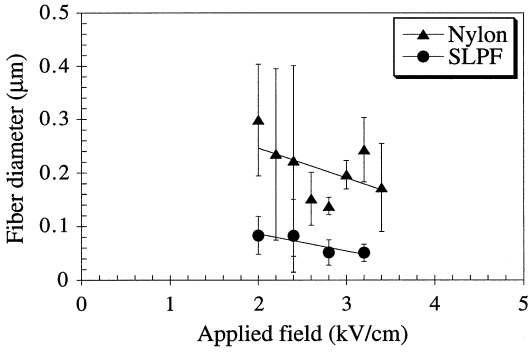

Fig. 4. Fiber diameter decreases with increasing applied field. The error bars indicate the large spread in sizes. The solution concentration was 12.1 wt.%.

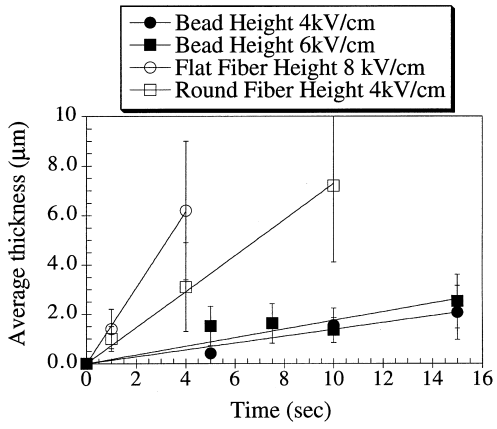

Fig. 5. Thickness of electrospun fibrous and beaded films increases with deposition time. Fibrous films deposited from conditions similar to beaded films tend to be thicker. The deposition rate is related to the slope of the lines and increases with applied field.

higher concentrations of 8.1 wt.% and above, there were evidently sufficient molecular chain entanglements in the polymer solution to prevent the breakup of the electrically driven jet and to allow the electrostatic stresses to further elongate the jet. Above 20 wt.%, the solutions became too viscous to be drawn into fibers before the dielectric breakdown of air took place. It is important to note that high viscosity fluids such as glycerol will form highly elongated jets when driven by an electric field [10]. Yet, monomeric fluids do not form solid fibers when electrospun. The same molecular response to elongational flow that makes conventional fiber formation from polymer solutions possible was apparently responsible for electrostatic fiber formation. However, when the concentration decreased, a gradual change in the morphology of the solid polymer took place in electrospinning that is not found in conventional fiber spinning.

Another morphological change occurred upon decreasing the distance between the syringe needle and the substrate. Regardless of the concentration of the polymer in the solution, low deposition distances corresponded to wet fibers or beads hitting the surface of the substrate. Fig. 3 illustrates the difference between the deposition distances of 0.5 and 2.0 cm. These observations were consistent with those described previously by Baumgarten [17] and Reneker and Chun [21]. The morphological result was that coating elements that look spherical were actually more like coins, and that cylinders were more like ribbons. The ratio of the height-to-width for wet-deposited coating elements was observed to be as low as 0.2. Wet coating elements coalesced while drying on the surface. This was analogous to thermal and solvent bonding in nonwoven polymeric fabrics [32]. Wet coating elements promoted intra- and inter-layer bonding.

In experiments evaluating the effect of deposition distance on morphology, the applied field was kept constant, that is, the applied voltage was proportionally decreased

Table 1
Critical voltage for electrospinning

Needle radius (cm)	Calculated kV	Observed kV
0.0076	1.5	3.7
0.0165	2.1	3.8
0.0292	2.6	4.2

with deposition distance. A series of experiments was carried out where the applied voltage was varied from 2 to 4 kV/cm and the deposition distance was held at 2 cm. Fig. 4 is a graph of one such experiment where the solution concentration was 12.1 wt.%. There was a decrease in fiber diameter with increasing applied electric fields. Increasing the field increased the electrostatic stresses on the jet, which was analogous to increasing the draw rate in conventional fiber spinning. This result was consistent with observations made by Larrondo and Manley [2]. Fig. 4 also shows a similar behavior for electrospun nylon. The error bars indicate the fairly large standard deviation in fiber or bead dimensions typical of the electrospinning process. For SLPF at these conditions, the spread averaged 35 nm, which was 55% of the average measured diameter of 64 nm, while the spread for nylon averaged 85 nm, which was 50% of the average diameter of 170 nm.

It was observed that the deposition rate increased as a function of the applied field. Fig. 5 is a graph of the increase in film thickness as a function of field for different electrospinning conditions. Beaded films deposited at 1 cm and at 4 or 6 kV/cm were approximately 1 μm thick after 10 s. In contrast, fibrous films deposited at 2.0 cm and 8 kV/cm were approximately 7 μm thick after 10 s.

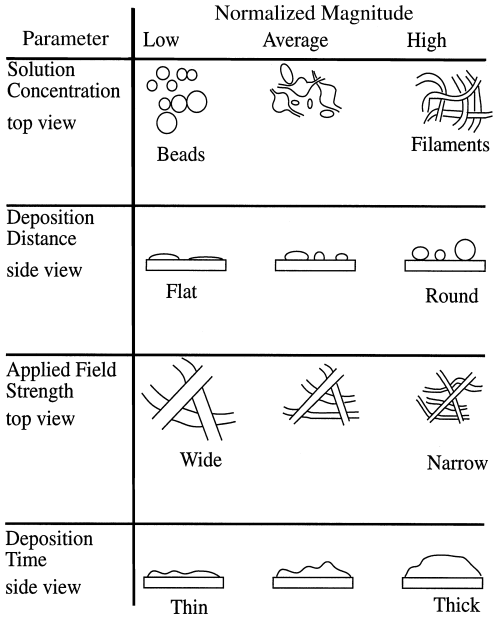

Fig. 6. Schematic of the effect of process parameters on film morphology. The process parameters of solution concentration, deposition distance, applied field strength, and deposition time can be combined to produce coatings with a variety of structures. The specific values for the parameters used in this study are included in Table 2.

The critical voltage required to initiate electrospinning was compared to the equations presented by Taylor [10] and Hendricks et al. [11]. In addition to the values of the syringe radius given in Table 1, the length of the capillary, *L*, was 1.8 cm, the separation between syringe and the ground, *H*, was 2.0 cm, and the surface tension of the solution was 37.1 dyn/cm for each measurement. The values obtained for different concentrations of polymer in solution were consistently higher than the calculated values (Table 1). The voltage required to initiate electrospinning increased slightly with concentration, despite the fact that surface tension changes only slightly with concentration [33]. This same observation was made by Doshi [19] which indicated that the solution viscosity plays a role in initial droplet deformation that was not adequately described by either Taylor [10] or Hendricks et al. [11].

The observations of the critical voltage required to initiate electrospinning were made using video microscopy. Using this setup, the nature of the cone and the length of the jet emanating from the tip of the cone could be observed. In contrast to the maximum jet length of 250 mm reported by Doshi [19] (for PEO in aqueous solutions) the maximum jet length observed for the SLPF/formic acid solution was 0.035 mm. Visually, the jet at the tip of the cone resembled a cloud of spray more than a single filament. This was probably because of the high instability of the jet at the cone tip, and was similar to modes of electrostatic atomization described elsewhere [9,13]. The length of the jet was shown to be influenced primarily by solution viscosity and conductivity [13]. The large dispersity in fiber diameters generated by the process was probably a result of this instability.

The effects on coating morphology of the four parameters, solution concentration, deposition distance, applied field strength and deposition time, are schematically represented in Fig. 6. By combining these four parameters, a wide variety of coating types could be produced. The absolute magnitudes of the parameters required to obtain a desired microstructure are interdependent. For example, reducing concentration to change the morphology from fiber to beads will have an effect on the range of applied fields required to change the average element size. Table 2 lists the range of values found in this system for the electrospinning parameters and the resulting structures. The crossover point from beads to filaments was between 6 and 8 wt.% for SLPF. The diameters depended somewhat on the deposition distance, as wet fibers or beads tend to spread out more when they hit the surface than dry fibers or beads. The height aspect ratio refers to the ratio between the thickness of a fiber or bead divided by its diameter. The lower thickness limit quoted for a 1 s deposition time was for the thinner beaded films, and the upper limit was for the thicker fibrous films (Fig. 5).

Now that we have established these relationships between electrospinning process parameters and the microstructure

Table 2
Relation of process parameters to structure variables

Process parameters		Structure variables	
Concentration	1.6–16 wt.%	Shape	Beads–filaments
Applied field strength	2–9 kV/cm	Diameter	2.0–0.20 μm
Deposition distance	0.5–4 cm	Height aspect ratio	0.2–1.0
Deposition time	1–15 s	Film thickness	0.1–15 μm

of the film, we can better predict the conditions required to make electrospinning possible given some knowledge of the solution properties of the desired polymer. Formic acid works well as the polymer solvent in this case because it is volatile (b.p. 100°C). A volatile solvent requires less deposition distance to form a solid product under ambient conditions. Lower deposition distances in turn require lower applied voltages to create sufficient field strength. In the case of aqueous polymer solutions, separation distances of ∽ 25 cm were required in order to collect dry filaments as compared to 2 cm in this case [19]. High viscosity polymer solutions also required higher electric fields than lower viscosity solutions.

3.2. Microstructure

Filaments of SLPF and nylon electrospun onto glass coverslips displayed oriented birefringence in the optical microscope. The light intensity was a maximum at 45° to the polarizer, and a minimum at 0° and 90° to the polarizer. The sign of the birefringence for the SLPF and nylon filaments was positive, which is typical of synthetic fibers and indicates that the index of refraction was larger along the fiber axis than in the lateral direction. Cast films of SLPF had spherulites and spherulitic structures consistent with those described by Anderson et al. [28], and the sign of the birefringence of these structures was negative. The magnitude of the birefringence for the nylon and SLPF fiber was estimated as 0.06 using the Michel–Lévy Color Chart and quartz wedge, which was consistent with reported values of 0.065 and 0.060, respectively [34]. Magoshi [35] correlated a negative birefringence in silk films with the Silk I. The crystal structure postulated for dry powder SLPF was a Silk I morphology.

The WAXS of cast nylon films showed crystalline diffraction peaks, but the scattering from the SLPF films was very diffuse (Fig. 7). The low crystallinity in the cast SLPF films was in contrast to the semi-crystalline diffraction seen in patterns of as-received SLPF powder [29]. The films used for WAXS were cast onto substrates and allowed to dry in air, and the final thickness of the films was on the order of 2 mm. The films observed in the optical microscope were cast onto a glass slide and covered with a coverslip. The films were analyzed after 2 h drying times and after drying overnight. While more birefringence developed in the thin optical samples, the diffraction patterns of the SLPF WAXS samples remained essentially the same. WAXS was also performed on electrospun nylon and SLPF thin films. Fig. 8 is WAXS of electrospun nylon and shows the same (2 0 0) and (0 0 2)/(2 0 2) peaks found in the WAXS of cast nylon. The film thickness was about 10 μm, based on calculations of the deposition rate.

Samples of SLPF thin films examined using a fiber diffraction apparatus showed a diffuse uniform ring at a d-spacing of 0.45 nm. These patterns confirmed a low crystallinity for electrospun SLPF thin films, but were not

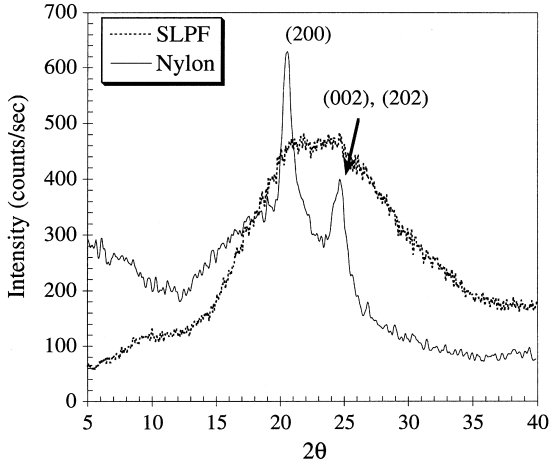

Fig. 7. WAXS patterns of cast films of nylon and SLPF. The patterns show crystalline peaks in the nylon films and a broad semi-crystalline halo in the SLPF.

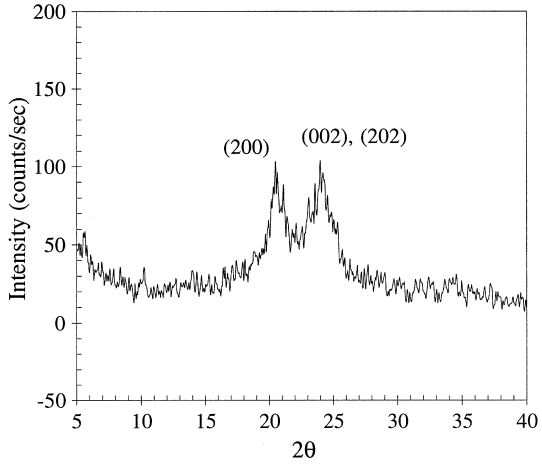

Fig. 8. WAXS patterns of electrospun nylon thin films. The same crystalline peaks seen in the WAXS patterns of cast nylon thin films are apparent in this pattern.

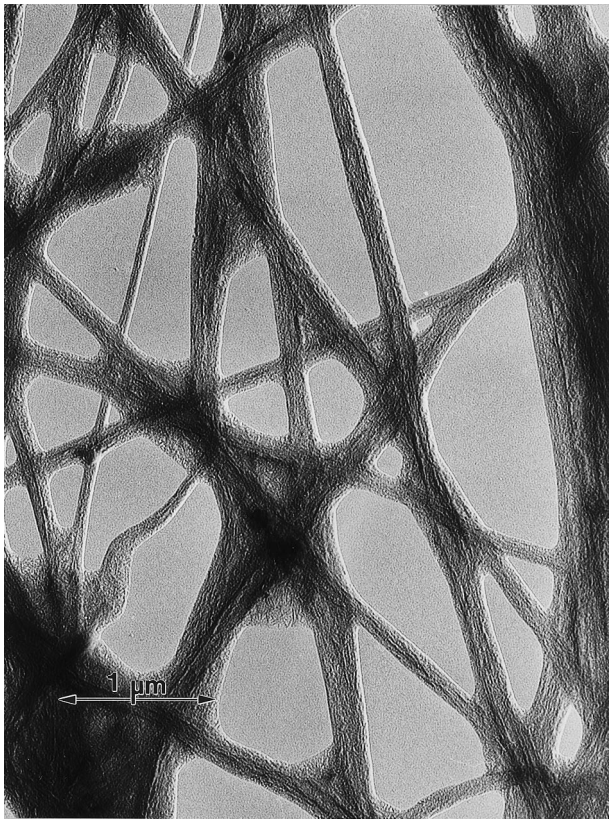

Fig. 9. The bright field TEM of electrospun SLPF filaments reveals a fibrillar texture. Crystallites can be seen at the thinnest parts of the filaments.

illustrative of the extent of molecular orientation owing to the random orientation of fibers in the film. TEM was used to evaluate the local molecular orientation in electrospun filaments.

TEM micrographs of nylon and SLPF showed a fibrillar texture in the filaments that was oriented along the fiber direction (Fig. 9). The fiber crossover points had a more randomly oriented texture. The wet fibers that resulted from a small deposition distance appeared to be bonded together at the junctions. The fibrillar surface texture was consistent with SPM studies of electrospun poly(ethylene oxide) fibers that were oriented at the surface in the fiber direction [30]. Whisker-like structures $\backsim$ 12 nm wide can be seen in Fig. 9 in the thinnest parts of the filaments. These were similar to those observed in TEM of atomized dilute solutions of SLPF [28].

Electron diffraction from nylon and SLPF thin films was observed in the TEM, as seen in Fig. 10. The nylon diffraction pattern is typical of oriented polymer fibers, with the lateral spacing of aligned molecules giving rise to the (2 0 0) equatorial reflections that have a d-spacing of 0.44 nm. The crystallite size was 10.5 nm and the misorientation angle was 17°. Samples of nylon electrospun at 3–5 kV/cm were examined in the TEM. The extent of orientation was not well-correlated with the applied field strength, and included diffuse rings and patterns similar to Fig. 10 in each sample.

Crystalline diffraction patterns were also observed in electrospun SLPF fibers (Fig. 10). The arcs of diffraction in Fig. 10 are consistent with a moderate molecular orientation in a polymer fiber and correspond to a d-spacing of 0.45 nm. The crystallite size was 11.5 nm and the misorientation angle was 35°. Water was added to 12.1 wt.% SLPF in formic acid at concentrations of 5%, 10% and 20% in an attempt to force the polymer in the solution closer to precipitation before electrospinning. Examination in the TEM revealed that the electrospun fibers containing 5% and 10% were morphologically and microstructurally similar to SLPF fibers spun from 100% formic acid. There was no apparent improvement in the crystallinity or orientation of these samples. The 20% water samples did not form fibers, indicating an upper limit for the amount of water tolerable to the electrostatic fiber formation process.

The results of the microstructural characterization of electrospun filaments can be compared to fibrillar microstructures found in other semi-crystalline polymers. Larrondo and Manley [12] identified a shish kebab morphology in electrospun 1% poly(ethylene) in paraffin. This type of structure was found to result from flow conditions imposed on the polymer solution, and typically comprised a chain-folded lamellae on a fibrillar backbone [36]. SLPF was designed to encourage chain-folding; a previous work has proposed a microstructure consisting of chain-folded Silk I crystallites [28]. Crystallites with a similar microstructure were identified in TEM samples of electrospun SLPF. The fibrillar texture of these samples was obvious in the TEM micrographs as well as SEM micrographs. Fig. 11 is a schematic of a shish kebab microstructure consistent with the observations made in this study. The fibrillar backbone may be Silk I or Silk II, as 0.45 nm reflections observed by electron diffraction could arise from the (1 1 0) planes of Silk I or the (0 2 0) planes of Silk II. However, Silk II is the form which is common in silk fibers. The lamellae on the backbone may be Silk I crystallites such as those found in the TEM micrographs. The entire fiber is covered by an amorphous layer of SLPF. An analysis of electrospun fibers of SLPF by TEM and electron diffraction may distinguish local differences along the filaments that support this hypothesis.

4. Conclusions

The electrospinning process is shown to produce protein polymer coatings with a wide range of morphologies. Control can be exerted over the morphology and thickness of the coatings by varying four process parameters: solution concentration, applied field strength, deposition distance, and deposition time. Combinations of these parameters could generate thin films with structural gradients. For example, electrospinning wet and then dry fibers would create a density gradient in the direction normal to the substrate surface. There is evidence in the literature and in

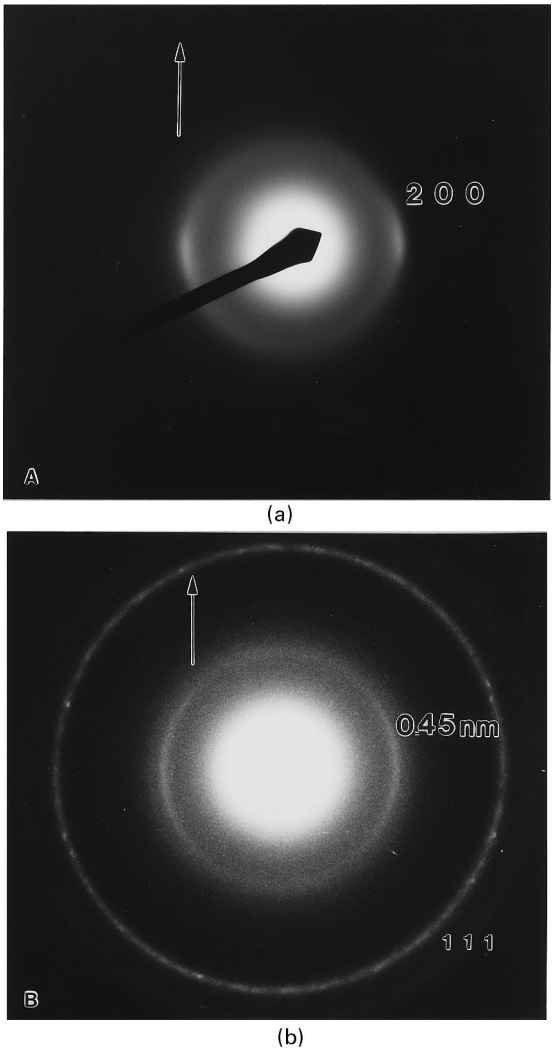

Fig. 10. Electron diffraction patterns of electrospun nylon and SLPF filaments. The arrow indicates the orientation of long direction of the fiber. (a) Arcs on the equator of the nylon diffraction pattern correspond to the (2 0 0) planes in the crystal. The crystallite size is 10.5 nm and the misorientation angle is 17°. (b) Arcs in the SLPF pattern correspond to a d-spacing of 0.45 nm and could be indexed as the (1 1 0) planes of Silk I or the (0 2 0) planes of Silk II. The crystallite size is 11.5 nm and the misorientation angle is 35°. The polycrystalline ring is the (1 1 1) reflection of gold, used as a calibration standard.

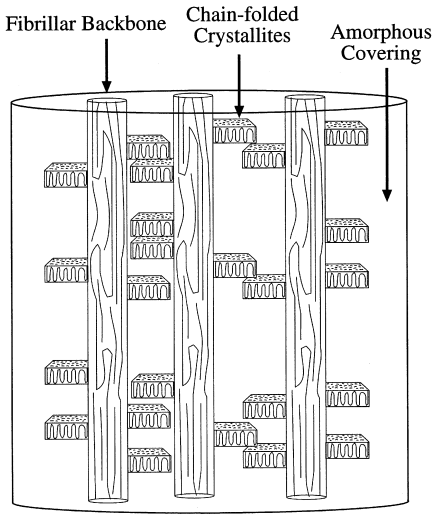

Fig. 11. Schematic of the shish kebab microstructure for electrospun SLPF. Electrospun filaments are composed of a backbone of microfibrils supporting chain-folded lamellar crystallites. The chain direction in the backbone and the lamellae is aligned with the fiber axis. For SLPF, the lamellae are probably Silk I, and the fibrillar backbone may be Silk I or Silk II. The Silk II crystal structure is commonly found in spun silk fibers. The shish kebabs are covered by an amorphous SLPF layer.

our lab for even more control over the deposition process. Transverse electrostatic fields can deflect charged droplets [19] and AC applied fields can influence the morphology in periodic ways, creating a variety of new shapes on the surface [33].

The electrospinning method used to generate thin, fibrous films of nylon and SLPF yielded textured fibers. Some of the nylon fibers displayed molecular orientation along the fiber axis, but the orientation of the fibers in a given sample was nonuniform. Electrospun SLPF thin films were not well-oriented but did show evidence of crystallinity, in the TEM, X-ray diffraction, and the optical microscope studies. The extent of crystallinity in both the cast and electrospun SLPF was lower than that found in the as-received powder by WAXS [28,29]. While the limited crystallinity of electrospun thin films may have been influenced by the rapid solidification brought about by the process, this does not explain the lack of crystallinity in cast thin films. Methods to increase the crystallinity of the thin films after processing, such as thermal or solvent annealing, could help identify the mechanism limiting the development of crystallinity. In addition, the details of the influence of formic acid on the structural stability of the polymer should be examined.

Given the limited crystallinity of the electrospun samples, it was not possible to determine if the extensional flow field created by the electrostatic field generated the Silk II crystal structure found in natural silk fibers or the Silk I structure found in unstressed silk films. The 0.45 nm spacing observed by electron diffraction is common to both Silk I and Silk II.

Typically, mechanical properties such as modulus improve with molecular orientation in polymer fibers. The weak orientation in the electrospun SLPF could predict low tensile strength. The mechanical properties of these coatings is examined in another study [37]. Chemical modifications or processing schemes that promote liquid crystalline phases in SLPF solutions could improve the molecular alignment in processed products. Although no conclusive evidence exists as yet for liquid crystallinity in SLPF/formic acid solutions [6], continued exploration of the phase diagram or addition of mesogens to the polymer backbone could help develop ordered phases in solution.

Acknowledgements

Financial support for this research was provided by the Whitaker Foundation, the National Institutes of Health, and the Marion Sarah Parker Scholars Program. Protein polymer materials were provided by Dr. Joseph Cappello, Research Director, Protein Polymer Technologies Inc. Flat-film X-ray diffraction assistance was provided by Dr. Brendan Foran.

References

[1] Cappello J, Crissman J, Dornan M, Mikolajczak M, Textor G, Marquet M, Ferrari F. Biotech Prog 1990;6:198–202.
[2] Buchko CJ. PhD Dissertation, Ann Arbor, MI: University of Michigan, 1997.
[3] Cappello J, McGrath KP. In: Kaplan D, Adams WW, Farmer B, Viney C, editors. Silk polymers, Am Chem Soc Proc, 544. Washington, DC: American Chemical Society, 1994. p. 311.
[4] Anderson JP, Nilsson SC, Rajachar RM, Logan R, Weissman NA, Martin DC. In: Alper M, Bayley H, Kaplan D, Navia M, editors. Biomolecular materials by design, Mat Res Soc Symp Proc, 330. Pittsburgh, PA: Materials Research Society, 1994. p. 171.
[5] Buchko CJ, Kozloff KM, Sioshansi A, O'Shea KS, Martin DC. In: Cotell CM, Meyer AE, Gorbatkin SM, Grobe GL, editors. Thin films and surfaces for bioactivity and biomedical applications, Mat Res Soc Symp Proc, 414. Pittsburgh, PA: Materials Research Society, 1996. p. 23.
[6] Martin DC, Jiang T, Buchko CJ. In: McGrath K, Kaplan D, editors. Protein-based materials. Boston, MA: Birkhauser, 1997, p. 339–370.
[7] Anderson JP. In McGrath K, Kaplan D, editors. Protein-based materials. Boston: Birkhauser, 1997, p. 371–423.
[8] Zeleny J. Phys Rev 1917;10:1–6.
[9] Michelson D. Electrostatic atomization. Bristol: Adam Hilger, 1990.
[10] Taylor G. Proc Roy Soc London A 1969;313:453–475.
[11] Hendricks CD, Carson RS, Hogan JJ, Schneider JM. AIAA J 1964;2(4):733–737.
[12] Larrondo L, Manley R. St John. J Poly Sci, Poly Phys Ed 1981;19:909–940.
[13] Cloupeau M, Prunet-Foch B. J Elect 1990;25:165–184.
[14] Rulison AJ, Flagan RC. Rev Sci Instr 1993;64(3):683–686.
[15] How TV. US Patent 4 552 707; 1985.
[16] Martin GE. US Patent 3 876 738; 1977.
[17] Baumgarten PK. J Coll and Int Sci 1971;36(1):71–79.
[18] Doshi J, Reneker DH. J Elect 1995;35(2–3):151–160.
[19] Doshi JN. PhD Dissertation, Akron, Ohio: University of Akron, 1994.
[20] Doshi J, Srinivasan G, Reneker DH. Polym News 1995;20:206–207.
[21] Reneker DH, Chun I. Nanotech 1996;7:216–223.
[22] Magoshi J, Magoshi Y, Nakamura S. Appl Polym Symp, No 41: US-Japan seminar on polymer liquid crystals. New York: Wiley, 1985. p. 187–204.
[23] Kaplan D, Adams WW, Farmer B, Viney C. Silk polymers. Am. Chem. Soc. Proc.. Washington, DC: American Chemical Society, 1994.
[24] Lotz B, Keith HG. J Mol Biol 1971;61:201–215.
[25] Kratky O, Schauenstein E, Sekora A. Nature 1950;165:319–320.
[26] Ambrose EJ, Bamford CH, Elliot A, Hanby WE. Nature 1951;168:264–265.
[27] Lotz B, Cesari FC. Biochemie 1979;61:205–214.
[28] Anderson JP, Cappello J, Martin DC. Biopolymers 1994;34(8):1049–1058.
[29] Anderson JP, Stephen-Hassard M, Martin DC. In: Kaplan D, Adams WW, Farmer B, Viney C, editors. Silk polymers, Am Chem Soc Proc, 544. Washington, DC: American Chemical Society, 1994. p. 137.
[30] Jaeger R, Schonherr H, Vancso GJ. Macromolecules 1996;29:7634–7636.
[31] Martin DC, Thomas EL. Polymer 1995;36(9):1743–1759.
[32] Kroschwitz JI. Polymers: fibers and textiles. New York: Wiley-Interscience, 1990.
[33] Johnson M. Unpublished data, 1996.
[34] Rochow TG, Tucker PA. Introduction to microscopy by means of light, electrons, X-rays, or acoustics. New York: Plenum Press, 1994.
[35] Magoshi J. Physical properties and structure of silk: 4. spherulites grown from aqueous solution of silk fibroin. Polymer 1977;18:643–646.
[36] Schultz J. Polymer materials science. Englewood Cliffs, NJ: Prentice-Hall, 1974.
[37] Buchko CJ, Kozloff KM, Slattery MJ, Martin DC. Manuscript in preparation.